Tunable luminous color of LEDs achieved through integrating reliable multilevel RRAM ⊘

Meng Qi ⓘ ; Liu Yang; Tao Sun ⓘ ; Runze Xu; Ziyu Lv ⓘ ; Ye Zhou ⓘ ; Su-Ting Han ✉ ⓘ

Check for updates

View Online   Export Citation

Articles You May Be Interested In

Intensity-modulated LED achieved through integrating p-GaN/n-ZnO heterojunction with multilevel RRAM

Appl. Phys. Lett. (November 2018)

Conductance quantization control and neuromorphic properties in Pt-nanoparticle incorporated HfAlO$_x$ alloy memristor

Appl. Phys. Lett. (November 2021)

Heterogeneous integrated InP/SiC high-performance multilevel RRAM

Appl. Phys. Lett. (February 2024)

Tunable luminous color of LEDs achieved through integrating reliable multilevel RRAM
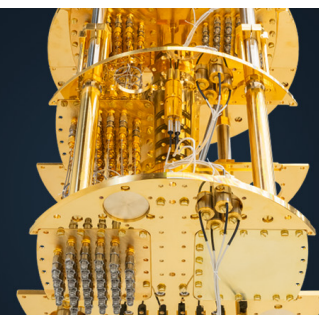
View Online   Export Citation   CrossMark

Meng Qi,[1] (iD) Liu Yang,[2] Tao Sun,[1] (iD) Runze Xu,[1] Ziyu Lv,[3] (iD) Ye Zhou,[4] (iD) and Su-Ting Han[5,a] (iD)

AFFILIATIONS

[1]Institute of Microscale Optoelectronics, Shenzhen University, Shenzhen 518060, People's Republic of China
[2]College of Science, Shenyang Aerospace University, Shenyang 110136, People's Republic of China
[3]College of Electronics and Information Engineering, Shenzhen University, Shenzhen 518060, People's Republic of China
[4]Institute of Advanced Study, Shenzhen University, Shenzhen 518060, People's Republic of China
[5]Department of Applied Biology and Chemical Technology, The Hong Kong Polytechnic University, Hung Hom, Kowloon,
Hong Kong, People's Republic of China

[a]Author to whom correspondence should be addressed: suting.han@polyu.edu.hk

ABSTRACT

We developed a color-modulated light-emitting device (LED) by the integration of a p-GaN/n-ZnO heterojunction with reliable resistive random access memory (RRAM) and demonstrated a multi-function integrated device with the adjustable electroluminescence (EL) color by modulating the injection current according to the multiple resistance states. As a critical foundation of an integrated device, reliable operation was achieved by introducing an AlO_x layer into HfO_x RRAM as an adjustment of the resistive switching endurance. Eventually, the EL color of LED was effectively regulated by modulating the compliance current of RRAM. Thanks to the high uniformity, this modulated LED may be a promising candidate for the application of low-cost and high-density LED displays without complicated structures and techniques, and it can provide a feasible approach for the realization of multilevel resistance state feedback from varied EL color in the future.

Published under an exclusive license by AIP Publishing. https://doi.org/10.1063/5.0226980

Developments of multifunctional integrated devices, including wearable devices, pressure sensors, and optical devices, have attracted extensive attention, with the aim of opening up new ways to practical applications.[1–3] The information communication and storage for the functional enhancement are at a stage of rapid development, which are now omnipresent and paramount.[4–6] Recently, an approach in the use of light-emitting devices (LEDs) integrated with resistive random access memory (RRAM) has been proposed.[7–9] LEDs without a doubt have various applications in the field of displays and lighting. However, these peripheral electronic devices of the actual application generally required complicated structures and fabrication techniques for controlling the electroluminescence (EL) color. It is worth noting that recent reports suggest that color-modulated LEDs can be developed by integrating with multilevel RRAM to take advantage of changes in resistance state.[7,10] Sun *et al.* reported the LED's illuminating color/intensity is switched by adjusting HRS and LRS, verifying the feasibility of regulation in LEDs.[10] Kratochvil *et al.* reported a device with adjustable color/intensity illuminating through the series connection of RRAMs and LEDs.[7] The fly in the ointment is that the integrated circuit requires eight RRAM devices in parallel, which is

relatively complicated for practical applications. For further development, there is an urgent need for multilevel RRAM and LED integration. Shan *et al.* recently reported that a brilliant job is to integrate the LEDs with multilevel RRAMs to achieve tunable EL intensity.[10] It is slightly unfortunate that the EL color modulation is not reversible. Consequently, there is a need to demonstrate more effective and feasible methods to achieve reversibly modulated LEDs as one critical issue of practical applications.

High reliability resistive switching (RS) behaviors of multi-level RRAM devices are the key factor of modulated LEDs. According to relevant literature reports, the RS mechanism of RRAM devices is based on the formation/rupture of nanoscale conductive filaments (CFs).[11–14] The fluctuation values of RS parameters are the decisive factor for the random microgeometry of CFs and RS location; overcoming these factors are a prerequisite for improving the RS uniformity.[15–18] Much work so far has focused on localizing the RS location, such as introducing metal nanoparticles, building a porous structure, and using a tip electrode.[15,19,20] Additionally, interest has been generated in the use of introducing active metal Al for RRAM devices that can improve the RS performance.[21–23] For instance, Chen *et al.* described better RS

uniformity by doping locally Al in HfO$_2$-RRAM;[21] Woo *et al.* demonstrated 12 distinct analog multilevel with an on/off ratio >10 by introducing Al in the RS layer;[22] Huang *et al.* reported an HfO$_2$/Al$_2$O$_3$ multilayer structure for RRAM arrays exhibiting outstanding retention characteristics.[23] However, reports on the aforementioned reliability devices showing the multifunctional behaviors are much less. Thus, inserting Al into the switching layer may provide a feasible approach for the realization of more reliable multilevel RS, enabling color modulation of LEDs with high accuracy in the integrated device.

In this work, we demonstrated color modulation of LEDs by integrating multilevel RRAMs with the structure Au/HfAlO$_x$/Au/p-GaN/ n-ZnO/In. Herein, the HfAlO$_x$ based RRAM devices presented highly reliable RS performance through doping Al in the storage layer. The devices exhibited uniformly multilevel RRAM by tuning compliance current (CC). Furthermore, the luminous color of the LEDs with the structure of Au/p-GaN/n-ZnO/In could be modulated by the injection current, which has preliminarily provided coherent feedback to certain resistance states. These findings may offer a route to develop reliable RRAMs with functional electronics.

First, we constructed the LED structure. The n-ZnO films were deposited on commercially available p-GaN:Mg (Mg $\sim$ 0.1 at. %) substrates by using an atomic layer deposition (ALD) method. Herein, the temperature of the grown ZnO films is 150 °C. The ZnO films with a thickness of $\sim$70 nm were obtained after 500 growth cycles. Then, metals Ni/Au and In circular pads were employed as the LED contact electrodes, respectively. Second, the Au/HfAlO$_x$/Au RRAM devices were established on the LEDs. The HfAlO$_x$ films were prepared by sequentially depositing AlO$_x$ and HfO$_x$ on Ni/Au contact electrodes of LEDs using ALD. The substrate temperature for the growth HfAlO$_x$ films and the films thickness were 250 °C and 10 nm, respectively. After that, the Au top electrodes with a diameter of 300 μm were directly deposited by evaporation process. Finally, as a comparison, the reference Au/HfO$_x$/Au RRAM devices without the AlO$_x$ layer were also fabricated in parallel. Electrical measurements were recorded using an Agilent B1500A semiconductor analyzer and all the tests were performed at room temperature.

Figure 1(a) presents the typical current–voltage (I–V) curves based on Au/HfAlO$_x$/Au devices. The bipolar RS behaviors was activated by utilizing a large voltage ($\sim$7 V) (see Fig. S1 in the supplementary material for forming curve). Subsequently, a CC of 1 mA was set to prevent permanent hard breakdown of RRAM devices. At positive sweep voltage (0–2 V), the device transitions to a low resistance state (LRS) from a high resistance state (HRS), which is responsible for the oxygen vacancies-based CFs.[24,25] The current rises suddenly at $\sim$1.5 V, which is defined as V$_{SET}$. At negative sweep voltage (0 to −2 V), oxygen vacancies recombine with oxygen ions to cause the rupture of CFs, allowing the devices to switch to the HRS. A sudden decline of the current occurred at $\sim$−0.8 V, which is defined as V$_{RESET}$. As shown in Fig. 1(b), alternating forward and reverse scan voltages were required to trigger repeated RS events under the 10^6 cycles. It is worth mentioning that the endurance of RRAM without AlO$_x$ collapses within the window of HRS/LRS for less than $\sim$10^5 RS cycles. The oxygen reservoir AlO$_x$ layer as a regeneration seed for CF may be the decisive factor for achieving good endurance (for more details, see Fig. S2 in the supplementary material).[26] The retention characteristics of both HRS and LRS are shown in Fig. 1(c). The LRS/ HRS values maintained high stability and did not exhibit failure for 10^5
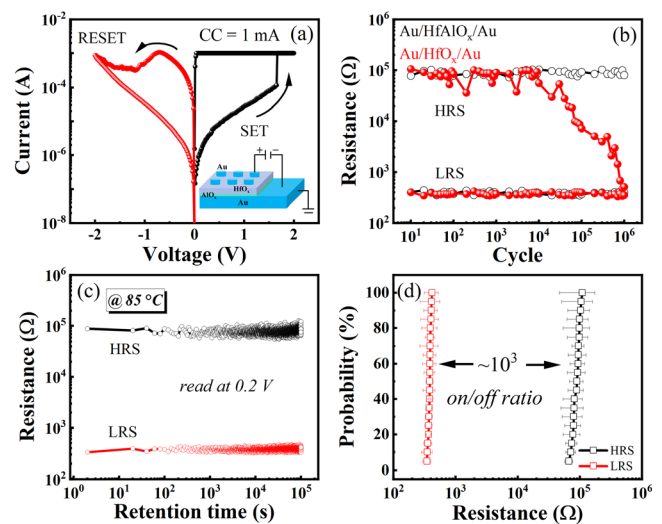

FIG. 1. (a) I–V curves of the Au/HfAlO$_x$/Au device. (b) Endurance and (c) retention characteristics of the Au/HfAlO$_x$/Au device. (d) Device-to-device variations in the distributions of HRS and LRS.

s at 85 °C. In addition, switching data of 20 random devices (each with 100 cycles) were collected to explore the fluctuation of RS between devices, as shown in Fig. 1(d). The on/off ratio up to $\sim$10^3 was obtained, which is responsible for the realization of multilevel memory without operation error. The acceptable distributions [standard deviations (σ)/mean value (μ)] indicate the potentiality to provide platforms for the development of multifunctional RRAM applications.

To gain clear insight into the properties of the integrated LED, we investigated RS reliability of the multilevel RRAM. The switching uniformity of the Au/HfAlO$_x$/Au device is of great importance for achieving the multilevel ability. Multilevel RRAMs were obtained by adjusting the CC to control the strength of CFs, as shown in Fig. 2(a). The LRS could be decreased from $\sim$10^3 Ω to $\sim$30 Ω as the CC increased from 1 to 20 mA. The HRS dependent variation curves of voltage stop were presented in the supplementary material (Fig. S3). These multilevel resistance states are clearly distinguishable by 100 switching cycles, indicating that the stable performance has the capability of avoiding misreads in adjacent states [Fig. 2(b)]. The cumulative probability of the multilevel LRS/HRS for the Au/HfAlO$_x$/Au RRAMs was acceptable variability in 28.2%, 29.7%, 30.2%, and 35.7% under the CCs of 20, 10, 5, and 1 mA, respectively, as shown in Fig. 2(c). The good reliability of HRS/LRS states indicates its strong potential for application as nonvolatile memristors and for LED integrated devices.

Furthermore, the electrical and optical properties of heterojunctions consisting of n-ZnO and p-GaN [Fig. 3(a)] was studied, as shown in Fig. 3. When conducting in the forward direction, a distinct rectification behavior emerges between the n-ZnO and p-GaN interface [Fig. 3(b)], while a favorable Ohmic contact is established in the In/n-ZnO and p-GaN/Au, as shown in the insertion in Fig. 3(b). The photoluminescence (PL) curves of the n-ZnO thin film and the p-GaN thin film are presented in Fig. 3(c). The black curve and red curve, respectively, represent the ZnO and GaN PL curve. The luminescence spectrum of ZnO exhibits two distinct emission bands centered at 380 and
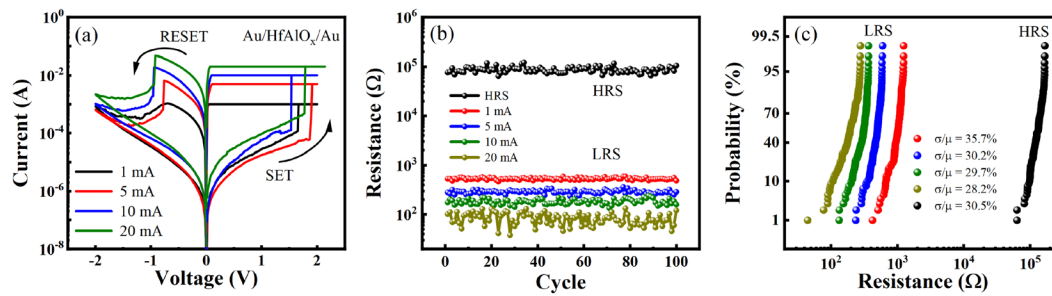
FIG. 2. (a) Multilevel characteristics of the Au/HfAlO$_x$/Au device by tuning the CC. (b) Evolution of HRS/LRS obtained under variable CCs. (c) Distribution of HRS/LRS collected from 500 switching cycles.

530 nm, respectively. The band located at 380 nm corresponds to the near-band edge (NBE) radiation, representing the radiative recombination within the ZnO.[27] The other band centered at 530 nm is attributed to defect-related radiative transitions, indicating the presence of imperfections or impurities within the ZnO lattice that act as luminescent centers.[28,29] Analyzing the PL curve of the p-GaN thin film reveals that the luminescent centers are situated at approximately 425 nm. This peak is attributed to the radiative transitions associated with an Mg acceptor in GaN.[30,31]

In addition, the EL curves of the n-ZnO/p-GaN heterojunction device under different currents are shown in Fig. 3(d). In the spectrum, it can be seen that the electroluminescence intensity significantly increases as the injection current increases under forward voltage. Compared with the PL curve in Fig. 3(c), the main peaks at ∼384 and ∼550 nm in the EL curve are derived from the NBE recombination

and defect-related radiation of ZnO, respectively. The main peak at 425 nm corresponds to the transition of the Mg acceptor in GaN (for details see Fig. S4 in the supplementary material).[32,33] To gain a deeper understanding of the electrons–holes recombination mechanism, the characteristics of the spectrum can be further explained by the energy band diagram in Fig. 3(e). Under forward bias conditions, electrons and holes are injected and tunnel through the small interface barrier between the GaN and ZnO layers. This allows the electrons to inject the GaN while the holes inject the ZnO. Consequently, radiative transitions result in emissions from both the n-ZnO and p-GaN, which are observed simultaneously. However, a crucial factor influencing the emission spectrum is the relatively higher concentration of defect/impurity levels in the low-temperature ALD-grown ZnO film.[34] As a result, the yellow-green light emission originating from the ZnO layer dominates the overall EL spectra because of the limited injected charge
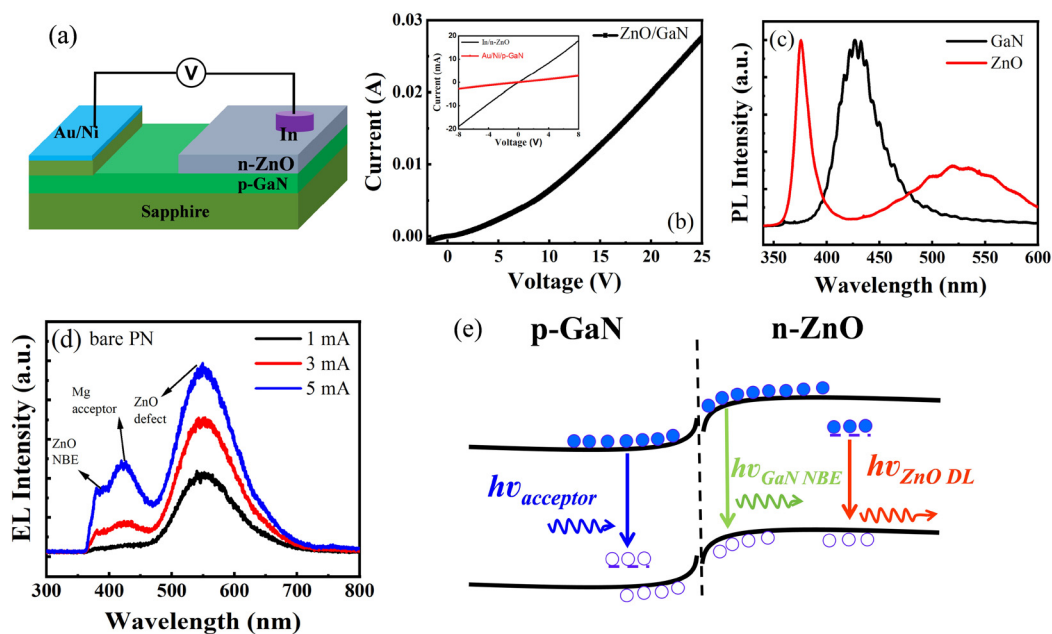
FIG. 3. (a) Schematic representation of the structural configuration of a p-GaN/n-ZnO LED. (b) The rectifying I–V curve of this PN junction device is depicted, with near-linear I–V curves of the p-GaN/Ni/Au and n-ZnO/In interfaces presented in the inset for reference. (c) PL spectra of p-GaN and n-ZnO film. (d) EL spectra of p-GaN/n-ZnO LED at different injection currents. (e) Energy band alignment of the p-GaN/n-ZnO heterojunction LED.
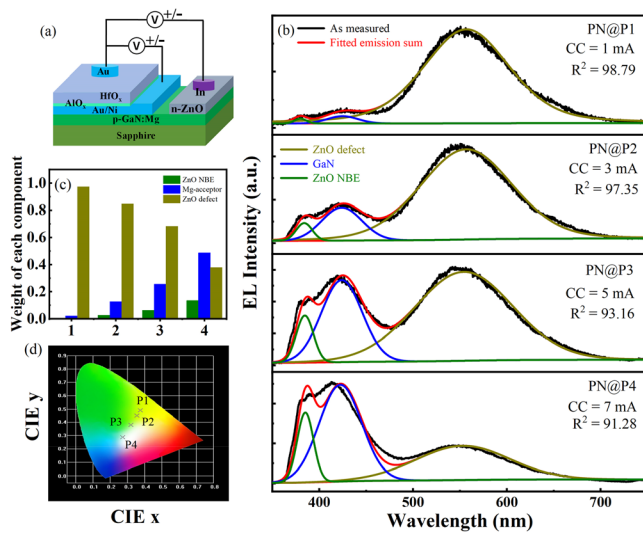
FIG. 4. (a) Schematic representation of the structural configuration of Au/HfAlO$_x$/Au/ p-GaN/n-ZnO/In. (b) Gaussian deconvolution fittings of the integrated devices with different CCs. (c) Relative spectral weight of three EL components. (d) CIE 1931 chromaticity diagram of integrated device operated at different CCs.

carriers captured by these defect/impurity energy levels (see Note 1 in the supplementary material, for discussion of EL emission from bare p-GaN/n-ZnO heterojunction). Therefore, detecting broadband visible light emission from the p-GaN/n-ZnO heterojunction LED provides significant potential for visually monitoring multi-level resistive states.

To integrate an LED with RRAM, we crafted a device architecture comprising Au/HfAlO$_x$/Au/p-GaN/n-ZnO/In, as depicted in Fig. 4(a). Within this configuration, the Au/HfAlO$_x$/Au segment serves as the

crucial functional layer responsible for the RS operations. The entire device acts as a dynamically modulated LED. Figure 4(b) exhibits the EL curves of the integrated devices, measured under the varying conditions of four distinct LRSs attained through adjustments in the CCs. The EL curve is decomposed into three prominent peaks at each current level by Gaussian deconvolution fitting [see Note 2 in the supplementary material for discussion of R-square (R^2) determined in the fitted emission sum], centered at approximately ∼384, ∼550, and ∼425 nm. Analysis of the PL curve suggests that these emission peaks correspond to the NBE recombination in ZnO, defect recombination within ZnO, and the Mg acceptor level recombination in GaN. Figure 4(c) reveals the evolving trend in the proportion of each component within the EL peak curve as the CC is incremented. Specifically, under conditions of low injection, the radiation recombination associated with defect energy levels in ZnO predominates. As the injection current intensifies, the NBE emission in ZnO gains prominence, becoming increasingly stronger. Owing to this evolving trend, the luminescence color exhibited by the n-ZnO/p-GaN heterojunction LED undergoes a shift, as depicted in the Commission Internationale de L'Eclairage (CIE) 1931 standard chromaticity diagram in Fig. 4(d). Initially, the color transitions from a yellow to a green emission, eventually culminating in the emission of white light. By integrating the functionalities of the LED and multilevel RRAMs, the spectra of the LEDs demonstrate an effective modulation of the luminous color.

In order to further exploit the potential applications of storage-display based RRAM, which maintains excellent performance at the multilevel resistive states, a 5 × 5 planar Au/HfAlO$_x$/Au/p-GaN/n-ZnO/In array was designed, as shown in Fig. 5(a). In Figs. 5(b) and 5(c), the resistance values of the RRAM device were measured after the SET and RESET process to ensure sure that the arrays were relatively uniform and could be in accord with the current densities of LED. Subsequently, the integrated arrays were stimulated by
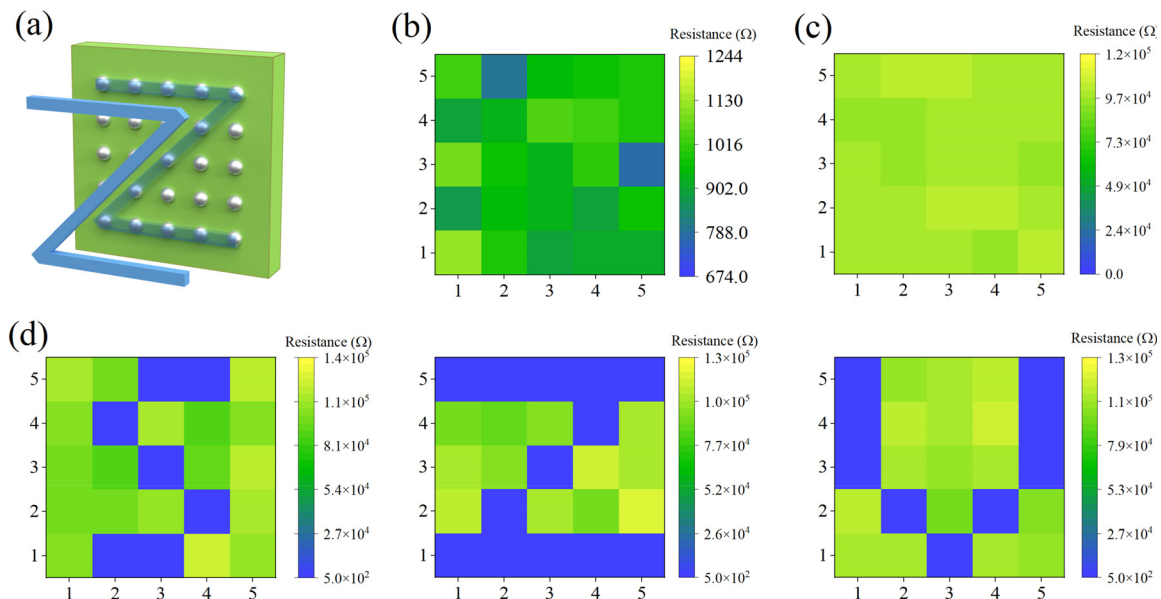

FIG. 5. (a) Illustration of optoelectronic and memorizing behaviors based on the integrated arrays design (5 × 5 arrays). (b) LRS and (c) HRS of the integrated devices array. (d) The resistance value of the integrated devices array at different CCs.

different CCs. In our architecture with reduced dimensionality, each letter of the "S, Z, U" has different resistive states corresponding to the optical characteristics of LED, which can be used for supervised storage status inputs [Fig. 5(d)]. It was obvious that planar integrated arrays exhibited significant recognition ability in multiple resistive states relying on its excellent storage and photosensitivity nature. The results indicate that the combination of memory and LED has good photoelectric response behavior, which is conducive to the construction of storage, computing, and display integrated devices, and has advantages in the integrated photoelectric systems.

In summary, we integrated the structure of Au/HfAlO$_x$/Au/p-GaN/n-ZnO/In for developing a color-tunable LED utilizing a multi-level RRAM device. The diverse color of LED could be modulated by adjusting the CCs of RRAM. This color-tunable LED might be adequate for low-cost and high-density LED displays to replace traditional selectors. Meanwhile, the color-tunable LEDs have capability of providing relational resistive feedback by the vision, indicating its potential for application in sensory-memory-display. In addition, the RRAM with more distinguished levels expected continues to be a great impetus to research efforts for the integrated devices with regulation of luminous color. These results might provide a feasible method for the development of functional electronic devices integrated with reliable RRAM.

See the supplementary material for detailed information on the forming curve; the RS mechanism; the relationship between voltage stops and HRS; the Mg acceptor-related emission mechanism; EL emission from bare p-GaN/n-ZnO heterojunction; and the R^2 determined in the fitted emission sum.

AUTHOR DECLARATIONS
Conflict of Interest

The authors have no conflicts to disclose.

Author Contributions

Meng Qi: Conceptualization (equal); Data curation (equal); Formal analysis (equal); Investigation (equal); Writing – original draft (equal). **Liu Yang:** Data curation (equal); Formal analysis (equal); Methodology (equal). **Tao Sun:** Data curation (equal). **Runze Xu:** Data curation (equal); Software (equal). **Ziyu Lv:** Supervision (equal). **Ye Zhou:** Funding acquisition (equal); Supervision (equal); Validation (equal). **Su-Ting Han:** Conceptualization (equal); Formal analysis (equal); Funding acquisition (equal); Supervision (equal); Validation (equal); Writing – review & editing (equal).

DATA AVAILABILITY

The data that support the findings of this study are available within the article and its supplementary material.

REFERENCES

[1] Y. Guo, F. Yin, Y. Li, G. Shen, and J.-C. Lee, Adv. Mater. **35**, 2300855 (2023).

[2] N. Liang, R. Tian, Y. Xu, H. Yao, H. Yang, Y. Wei, X. Xin, R. Chen, T. Zhai, Z. Wang, and J. Hou, Adv. Mater. **35**, 2300360 (2023).

[3] X. Xiong, J. Liang, and W. Wu, Nano Energy **113**, 108542 (2023).

[4] H. Li, H. Gong, T. H. Wong, J. Zhou, Y. Wang, L. Lin, Y. Dou, H. Jia, X. Huang, Z. Gao, R. Shi, Y. Huang, Z. Chen, W. Park, J. Y. Li, H. Chu, S. Jia, H. Wu, M. Wu, Y. Liu, D. Li, J. Li, G. Xu, T. Chang, B. Zhang, Y. Gao, J. Su, H. Bai, J. Hu, C. K. Yiu, C. Xu, W. Hu, J. Huang, L. Chang, and X. Yu, Nat. Commun. **14**, 7539 (2023).

[5] A. O. Omoniyi, Y. Wang, S. Yang, J. Liu, J. Zhang, and Z. Su, Mater. Today Commun. **36**, 106508 (2023).

[6] G. Zhou, J. Li, Q. Song, L. Wang, Z. Ren, B. Sun, X. Hu, W. Wang, G. Xu, X. Chen, L. Cheng, F. Zhou, and S. Duan, Nat. Commun. **14**, 8489 (2023).

[7] S. Nau, V. B. Sørdal, C. Wolf, S. Sax, and E. J. W. List-Kratochvil, Appl. Phys. Lett. **107**, 133301 (2015).

[8] J. L. Zhao, K. L. Teo, K. Zheng, and X. W. Sun, Nanotechnology **27**, 115204 (2016).

[9] M. Qi, X. Zhang, L. Yang, Z. Wang, H. Xu, W. Liu, X. Zhao, and Y. Liu, Appl. Phys. Lett. **113**, 223503 (2018).

[10] X. Yang, C. Shan, Q. Liu, M. Jiang, Y. Lu, X. Xie, B. Li, and D. Shen, ACS Photonics **5**, 1006 (2018).

[11] R. Waser, R. Dittmann, G. Staikov, and K. Szot, Adv. Mater. **21**, 2632 (2009).

[12] A. Wedig, M. Luebben, D.-Y. Cho, M. Moors, K. Skaja, V. Rana, T. Hasegawa, K. K. Adepalli, B. Yildiz, R. Waser, and I. Valov, Nat. Nanotechnol. **11**, 67 (2016).

[13] G.-S. Park, Y. B. Kim, S. Y. Park, X. S. Li, S. Heo, M.-J. Lee, M. Chang, J. H. Kwon, M. Kim, U. I. Chung, R. Dittmann, R. Waser, and K. Kim, Nat. Commun. **4**, 2382 (2013).

[14] M. Qi, Y. Tao, Z. Wang, H. Xu, X. Zhao, W. Liu, J. Ma, and Y. Liu, Appl. Surf. Sci. **458**, 216 (2018).

[15] Y. Tao, X. Li, Z. Wang, H. Xu, W. Ding, J. Ma, and Y. Liu, Appl. Phys. Lett. **111**, 183504 (2017).

[16] S. Gao, G. Liu, Q. Chen, W. Xue, H. Yang, J. Shang, B. Chen, F. Zeng, C. Song, F. Pan, and R.-W. Li, ACS Appl. Mater. Interfaces **10**, 6453 (2018).

[17] D. Yang, J. Xue, J. Wang, H. Wang, S. Wang, X. Lei, J. Yan, and W. Zhao, ACS Appl. Electron. Mater. **6**, 4764 (2024).

[18] Y. Tao, W. Ding, Z. Wang, H. Xu, X. Zhao, X. Li, W. Liu, J. Ma, and Y. Liu, Appl. Surf. Sci. **440**, 107 (2018).

[19] M. Qi, S. Cao, L. Yang, Q. You, L. Shi, and Z. Wu, Appl. Phys. Lett. **116**, 163503 (2020).

[20] L. Wang, Y. Wang, and D. Wen, J. Alloy. Compd. **892**, 162180 (2022).

[21] Y. S. Chen, B. Chen, B. Gao, L. F. Liu, X. Y. Liu, and J. F. Kang, J. Appl. Phys. **113**, 164507 (2013).

[22] J. Woo, K. Moon, J. Song, S. Lee, M. Kwak, J. Park, and H. Hwang, IEEE Electron Device Lett. **37**, 994 (2016).

[23] X. Huang, H. Wu, G. Bin, D. C. Sekar, L. Dai, M. Kellam, G. Bronner, N. Deng, and H. Qian, Nanotechnology **27**, 395201 (2016).

[24] J. Zhang, F. Wang, C. Li, X. Shan, A. Liang, K. Hu, Y. Li, Q. Liu, Y. Hao, and K. Zhang, Appl. Surf. Sci. **526**, 146723 (2020).

[25] B. Traore, P. Blaise, B. Sklénard, E. Vianello, B. Magyari-Köpe, and Y. Nishi, IEEE Trans. Electron Devices **65**, 507 (2018).

[26] J. Liu, H. Yang, Y. Ji, Z. Ma, K. Chen, X. Zhang, H. Zhang, Y. Sun, X. Huang, and S. Oda, Nanotechnology **29**, 415205 (2018).

[27] X. Huang, L. Zhang, S. Wang, D. Chi, and S. J. Chua, ACS Appl. Mater. Interfaces **8**, 15482 (2016).

[28] H. Zhu, C.-X. Shan, B. Yao, B.-H. Li, J.-Y. Zhang, Z.-Z. Zhang, D.-X. Zhao, D.-Z. Shen, X.-W. Fan, Y.-M. Lu, and Z.-K. Tang, Adv. Mater. **21**, 1613 (2009).

[29] H. Zeng, G. Duan, Y. Li, S. Yang, X. Xu, and W. Cai, Adv. Funct. Mater. **20**, 561 (2010).

[30] Z. Guo, H. Li, L. Zhou, D. Zhao, Y. Wu, Z. Zhang, W. Zhang, C. Li, and J. Yao, Small **11**, 438 (2015).

[31] X. Fang, Z. Wei, Y. Yang, R. Chen, Y. Li, J. Tang, D. Fang, H. Jia, D. Wang, J. Fan, X. Ma, B. Yao, and X. Wang, ACS Appl. Mater. Interfaces **8**, 1661 (2016).

[32] P. Felbier, J. Yang, J. Theis, R. W. Liptak, A. Wagner, A. Lorke, G. Bacher, and U. Kortshagen, Adv. Funct. Mater. **24**, 1988 (2014).

[33] C. P. Chen, M. Y. Ke, C. C. Liu, Y. J. Chang, F. H. Yang, and J. J. Huang, Appl. Phys. Lett. **91**, 091107 (2007).

[34] L. Yang, W. Liu, H. Xu, J. Ma, C. Zhang, C. Liu, Z. Wang, and Y. Liu, J. Mater. Chem. C **5**, 3288 (2017).